Chemical Thermodynamics and Thermal Analysis 8 (2022) 100091

Contents lists available at ScienceDirect

Chemical Thermodynamics and Thermal Analysis

journal homepage: www.elsevier.com/locate/ctta

A comparative study of experiments and theories on steady-state evaporation of water

Michael T. Rauter[a], Ailo Aasen[a,b], Signe Kjelstrup[a], Øivind Wilhelmsen[a,*]

[a] PoreLab, Department of Chemistry, Norwegian University of Science and Technology, Trondheim 7491, Norway
[b] PoreLab, SINTEF Energy Research, Trondheim 7491, Norway

ARTICLE INFO

Keywords:
Evaporation
Interfaces
Water
Resistance
Experiments
Theory

ABSTRACT

A precise description of energy and mass transport across the liquid-vapor interface of water is central in disciplines spanning from climatology to seawater desalination. We present a critical assessment of six recent experimental data sets that report temperature jumps, vapor pressures, and evaporation rates during steady-state evaporation of water. The experimental data were used to test available theories. Three state-of-the-art theories that take the resistance of the liquid-vapor interface into account were compared; statistical rate theory, non-equilibrium thermodynamics, and kinetic theory of gases. Statistical rate theory appears to under-predict the difference between the saturation pressure and the actual pressure of the vapor phase. Interface transfer coefficients for water compatible with non-equilibrium thermodynamics theory were determined. These coefficients predict the right order of magnitude of the evaporation fluxes from the different data sets. However, inconsistencies between the different data sets and indications of systematic measurement errors were identified during the determination and evaluation of these coefficients. The condensation coefficient in kinetic theory of gases computed from the experimental data span two orders of magnitude. All three theories were found to depend much on a precise determination of the conditions at the interface, in particular on the difference between the vapor phase pressure and the saturation pressure. Already a shift of 1–5 Pa changes the predicted evaporation rates significantly. For certain experiments, a change of 2 Pa modifies the evaporation rate predicted by statistical rate theory by one order of magnitude. Overall, we show that determination of vapor pressures to a higher accuracy (<0.3 Pa) is needed to enhance the understanding of evaporation mechanisms and which theory to use.

1. Introduction

Evaporation and condensation of water is ubiquitous in nature and of great importance to many fields like climatology [1], seawater desalination [2], agriculture [3] as well as to numerous industrial applications [4–6]. One of the most frequently used ways to generate electricity is by steam turbines, and this involves phase change of water in every cycle [6]. In climatology, a correct description of evaporation and condensation is crucial for precise climate models, on the local as well as the global scale [1]. Phase transitions take place in seawater desalination technologies like membrane distillation [7,8] and flash evaporation [9]. It has therefore since long been of interest to understand the mechanisms involved, in order to improve weather forecasts, enhance evaporation rates in steam turbine cycles, or reduce energy needs in distillation columns. At the most fundamental level, the basis for such improvements lies in a precise description of mass- and energy transport across the liquid-vapor interface, in particular of water.

Mass transport across the liquid-vapor interface is frequently described, assuming a uniform temperature across the interface and with the vapor pressure equal to the equilibrium saturation pressure [10,11]. This, however, neglects the resistance of the interface itself and contradicts observations of temperature jumps at the liquid-vapor interface during steady-state evaporation of water [12–14]. Here, temperature jumps as large as 27.83 K have been reported [12]. Several studies have demonstrated that the interface resistances should be included for a precise local description of phase transitions in distillation columns [15,16] or membrane distillation processes [8,17]. Interface transport is also essential for a precise description of transport on the nanoscale, where curvature effects can alter the interface resistances by up to one order of magnitude [18,19].

Since the first experiments of Ward and Fang [20,21], there have been many experimental efforts aimed at mapping the characteristics of steady-state evaporation of water [12–14,22–24]. The experiments differ by many factors, such as the induced energy fluxes and the obtained evaporation rates. Most of the experiments have been performed for pure water in the supercooled regime, which is known to exhibit anomalous behavior compared to other fluids [25]. The determination of experimental values such as the vapor phase pressure or the heat fluxes has been prone to large statistical uncertainties [13,26]. Also,

* Corresponding author.
E-mail address: oivind.wilhelmsen@ntnu.no (Ø. Wilhelmsen).

https://doi.org/10.1016/j.ctta.2022.100091
Received 21 July 2022; Received in revised form 19 September 2022; Accepted 17 October 2022

systematic measurement errors close to the liquid-vapor interface have been discussed [27]. Steady-state water evaporation experiments, recently presented by Kazemi and Ward [14], have to the best of our knowledge, the highest accuracy reported to date. The collected experimental data now spans a wide range of measured fluxes and temperature jumps. This provides an excellent opportunity to evaluate their consistency, compare the data to other evaporation experiments in the literature [13,22–24], and assess available theories.

Steady-state evaporation of water has frequently been described by kinetic theory of gases (KTG), statistical rate theory (SRT) and non-equilibrium thermodynamics (NET) [20,28,29]. All three theories have in common that they predict a net mass flux across the vapor-liquid interface if there is a non-uniform temperature across the interface and/or if the vapor pressure deviates from the equilibrium saturation pressure. KTG has been used for more than a century to predict evaporation rates. The arguably most famous expression is the Hertz-Knudsen (HK) equation [30]. The theory makes use of evaporation- and condensation coefficients that describe the fraction of molecules that undergo a phase change from liquid to vapor and vice versa [31]. They are usually determined by comparison to experiments since no commonly acknowledged expression is available [30]. So far, the HK formula has been shown to give inaccurate and inconsistent predictions [30]. Experiments with water have resulted in condensation coefficients that differ by several orders of magnitude [30]. Another subject of criticism is that the HK equation does not satisfy momentum and energy balances for the interface transport [32]. We will reassess these findings in the present work and compare two expressions that originate from the HK equation to recent experimental data.

In SRT, introduced by Ward and Fang [20], the evaporation rate is calculated by use of transition probabilities between quantum mechanical states. The flux of molecules going from one phase to the other is related to the transition probabilities in both directions [14]. SRT applies to all fluids, and no fitting parameters are needed. It is in that sense a general theory. But the theory does not provide an expression for the energy flux across the interface. Such a description is important since evaporation is also driven by the temperature difference [33].

The energy- and mass fluxes across the interface are contained in the framework of NET, which consistently accounts for the coupling and interaction between the independent fluxes [29,34]. A shortcoming is that NET contains three unknown coefficients of transfer. While coefficients for NET have been determined for the whole temperature range relevant for evaporation/condensation of water, an independent assessment of the coefficients was only possible for the resistance to heat transfer [26]. We shall here compare the ability of SRT and NET to predict evaporation (mass fluxes) for varying experimental conditions. Special emphasis will be devoted to the role of the vapor pressure, i.e. the deviation of this pressure from the pressure at saturation. All theories, KTG, SRT, and NET, have been used to describe steady-state evaporation of water. However, there is still no consensus on which theory to prefer. This is not only due to the shortcomings of the theories discussed above, but also due to systematic and unsystematic uncertainties in the experimental data.

In this work we shall critically assess six different experimental data sets containing in total 159 single experiments [13,14,22–24] and evaluate their consistency. The different data sets will be used to compare and assess the three state-of-the-art theories. We review the essentials of the three theories in question in Section 2. Post-processing of experimental data and evaluation procedures are described in Section 3. We start with a preliminary discussion of the experimental data in Section 4, before the results are presented in Section 5. Concluding remarks are given in Section 6.

2. Theory

The aim of this section is to provide sufficient background on the three theories that will be discussed, SRT, NET, and KTG. We refer to Ward and Fang [20], Kjelstrup and Bedeaux [29] and to Persad and Ward [30] for further details of SRT, NET and KTG, respectively.

The fluxes across the interface must obey the mass-, energy- and momentum- balances for transport across the interface. At steady-state and for one-dimensional transfer perpendicular to the surface, the following fluxes across the interface are constant:

$$\rho^l v^l = \rho^g v^g = J \tag{1}$$

$$\rho^l (v^l)^2 + p_\perp^l = \rho^g (v^g)^2 + p_\perp^g = J_m \tag{2}$$

$$J_q'^{,l} + J(h^l + \frac{(v^l)^2}{2}) = J_q'^{,g} + J(h^g + \frac{(v^g)^2}{2}) = J_q \tag{3}$$

where J is the mass flux, ρ the density, v the velocity, $p_\perp$ the pressure perpendicular to the interface, J_m the momentum flux, J_q' the measurable heat flux, h the enthalpy and J_q the total energy flux. The liquid- and the gas side of the interface are indicated by superscript l and g, respectively. The kinetic energy contribution can often be neglected, and the measurable heat fluxes, J_q', are given in terms of the total energy flux, J_q, and the mass flux, J, by

$$J_q'^{g} = J_q - J h^g, \tag{4}$$

$$J_q'^{l} = J_q - J h^l, \tag{5}$$

$$J_q'^{g} = J_q'^{l} + J(h^g - h^l), \tag{6}$$

Eqs. 1 to 6 are common to all theories.

2.1. Statistical rate theory

SRT was developed in order to describe particle transport across an interface between two adjacent phases [35] and has for example been examined for gas sorption, chemical reactions and ion transport [30]. The expressions for the description of the mass flux during evaporation using SRT were introduced by Ward and Fang [20]. SRT can be used for the description of the evaporation flux for various fluids once the molecular and fluid properties are known [30]. Here we present the final form of the equations, following Kazemi and Ward [14]. The mass flux for evaporation, J_{SRT}, as predicted by SRT, is

$$J_{\mathrm{SRT}} = 2K_e X, \tag{7}$$

where K_e is the equilibrium molecular exchange rate and X is the exchange probability. In SRT the exchange probability is determined by the entropy change between the liquid and the vapor by

$$X = \sinh\left[\frac{\Delta s_{LV}}{k_B}\right]. \tag{8}$$

Here, Δs_{LV} is the deviation of the entropy difference between the liquid and vapor phase from equilibrium and k_B is the Boltzmann constant. Using classical kinetic theory, the equilibrium molecular exchange rate between the phases can be expressed as

$$K_e = \eta p_{\mathrm{sat}}(T^l)\sqrt{\frac{m}{2\pi k_B T^l}}, \tag{9}$$

where m is the molecular mass, p_{sat} is the saturation pressure at the temperature of the liquid and η accounts for curvature effects on the saturation values which can be determined using the Laplace equation (see [14]). The change in entropy from liquid to vapor can be split into three terms

$$\frac{\Delta s_{LV}}{k_B} = \frac{\Delta s_c}{k_B} + \frac{\Delta s_T}{k_B} + \frac{\Delta s_\omega}{k_B}, \tag{10}$$

where Δs_c is the configurational term, Δs_T the temperature discontinuity term and Δs_ω is the internal molecular-vibration frequency term.

Following the procedure by Kazemi and Ward [14], the three terms on the right-hand side of Eq. 10 can be expressed as:

$$\frac{\Delta s_c}{k_B} = \ln\left(\frac{p_{\text{sat}}(T^l)}{p^g}\right) + \frac{m v_f(T^l)}{k_B T^l}\left(p^g + \gamma^{LV} C - p_{\text{sat}}(T^l)\right), \tag{11}$$

$$\frac{\Delta s_T}{k_B} = 4\left(1 - \frac{T^g}{T^l}\right) + \ln\left(\frac{T^g}{T^l}\right)^4, \tag{12}$$

$$\frac{\Delta s_\omega}{k_B} = \ln\left(\frac{q^v_{vib}}{q^l_{vib}}\right) + \left(\frac{1}{T^g} - \frac{1}{T^l}\right)\sum_{i=1}^{\text{DOF}}\left(\frac{\theta_i}{2} + \frac{\theta_i}{e^{\frac{\theta_i}{T^g}} - 1}\right), \tag{13}$$

where v_l is the specific saturation volume of the liquid, C is the principal curvature and γ^{lv} is the liquid-vapor surface tension. The vibration partition function is given by:

$$q_{vib}(T) = \prod_{i=1}^{\text{DOF}} \frac{e^{-\theta_i/2T}}{1 - e^{-\theta_i/T}}, \tag{14}$$

where DOF is the vibrational frequency degree of freedom. The characteristic temperature of water molecules provided by Kazemi and Ward [14] are $\theta_1 = 5254$ K, $\theta_2 = 5405$ K and $\theta_3 = 2288$ K.

Eq. 7 reduces after simplifying assumptions to an expression similar to the HK equation with explicit expressions for the evaporation and condensation coefficients [30]. The condensation and evaporation coefficients are:

$$\sigma_e^* = \frac{p_{\text{sat}}(T^l)}{p^g}\exp\left[(\text{DOF}+4)\left(1 - \frac{T^g}{T^l}\right)\right]\left(\frac{T^g}{T^l}\right)^{\text{DOF}+4}, \tag{15}$$

$$\sigma_c^* = \sqrt{\frac{T^g}{T^l}}\exp\left[-(\text{DOF}+4)\left(1 - \frac{T^g}{T^l}\right)\right]\left(\frac{T^g}{T^l}\right)^{\text{DOF}+4}. \tag{16}$$

2.2. Non-equilibrium thermodynamics

Transport of mass and heat across the liquid-vapor interface can be described using NET, which is a theory that describes transport across interfaces without knowledge of the transfer coefficients. We present two alternative and equivalent formulations, based on the measurable heat flux of the gas phase or the liquid phase. The variables in Eqs. 4–5 are illustrated in Fig. 1 for a hypothetical enthalpy profile across the interface. The interfacial region is defined to start when the thermodynamic properties start to deviate from the respective bulk values of the liquid- or vapor phase (grey areas in Fig. 1).

The total energy flux and the mass flux are constant during steady-state evaporation. The measurable heat flux, however, depends on the local enthalpy, i.e. the measurable heat flux on the vapor side of the interface differs from the one on the liquid side of the interface, cf. Eq. 6. This implies that also the transfer coefficients depend on whether the force-flux equations are evaluated with the measurable heat flux on the vapor- or the liquid side of the interface. We shall in the following refer to the coefficients from NET that correspond to the measurable heat flux on the liquid side as the *liquid-side coefficients* and the coefficients that correspond to the measurable heat flux on the vapor-side as *vapor-side coefficients*. Note that both the liquid- and vapor-side coefficients apply to the whole interface. The force-flux equations for the measurable heat flux on the vapor side, $J_q'^g$, are

$$\begin{aligned} X_q &= R_{qq} J_q'^g + R^g_{q\mu} J, \\ X^g_\mu &= R^g_{\mu q} J_q'^g + R^g_{\mu\mu} J, \end{aligned} \tag{17}$$

where the left-hand-side contains the forces and the right-hand-side contains the fluxes. Choosing the measurable heat flux on the liquid side, $J_q'^l$, results in the following *alternative* force-flux relations

$$\begin{aligned} X_q &= R_{qq} J_q'^l + R^l_{q\mu} J, \\ X^l_\mu &= R^l_{\mu q} J_q'^l + R^l_{\mu\mu} J. \end{aligned} \tag{18}$$

Here, X_q is the driving force due to a temperature difference, X^g_μ and X^l_μ are the driving forces due to a difference in chemical potential, and R_{ij} are the overall interface transfer coefficients [29]. While the main resistance to heat transfer, R_{qq}, is independent of whether the force-flux relations are evaluated with the vapor- or liquid side measurable heat flux, the two coupling coefficients, $R_{q\mu} = R_{\mu q}$ [36,37]and the resistance to mass transfer, $R_{\mu\mu}$, are not. Using that the entropy production must be invariant with respect to the choice of force-flux formulation, the coefficients can be converted from one side to the other by:

$$R^l_{qq} = R^g_{qq} = R_{qq}, \tag{19}$$

$$R^l_{q\mu} = R^l_{\mu q} = R^g_{\mu q} - \Delta h_{vap} R^g_{qq}, \tag{20}$$

$$R^l_{\mu\mu} = R^g_{\mu\mu} - 2\Delta h_{vap} R^g_{q\mu} + (\Delta h_{vap})^2 R^g_{qq}, \tag{21}$$

for a conversion from the gas-side- to the liquid-side coefficients and by

$$R^g_{q\mu} = R^g_{\mu q} = R^l_{\mu q} + \Delta h_{vap} R^l_{qq}, \tag{22}$$

$$R^g_{\mu\mu} = R^l_{\mu\mu} + 2\Delta h_{vap} R^l_{q\mu} + (\Delta h_{vap})^2 R^l_{qq}, \tag{23}$$

for a conversion from the liquid-side- to the gas-side coefficients. The coefficients are related by the enthalpy of evaporation, Δh_{vap}.

2.2.1. The thermodynamic driving forces

The thermal driving force is:

$$X^g_q = X^l_q = X_q = \frac{1}{T^g} - \frac{1}{T^l}. \tag{24}$$

Here, T^l and T^g are obtained by extrapolating the temperature profiles from the bulk liquid and vapor phases to the defined dividing surface [29]. The driving force due to a difference in chemical potential must be evaluated at the temperature of the vapor phase, when the measurable heat flux is determined on the liquid-side:

$$X^l_\mu = -\frac{1}{T^g}\left(\mu^g(T^g) - \mu^l(T^g)\right), \tag{25}$$

$$= -\left(\frac{\mu^g(T^g)}{T^g} - \frac{\mu^l(T^l)}{T^l}\right) + h^l\left(\frac{1}{T^g} - \frac{1}{T^l}\right), \tag{26}$$

$$\approx -R_w \ln\left(\frac{p^g}{p_{\text{sat}}(T^g)}\right). \tag{27}$$

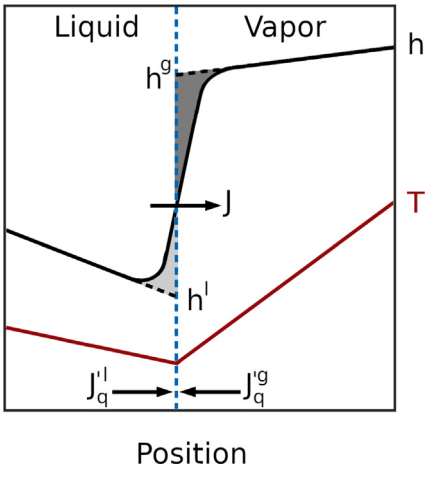

Fig. 1. An example of enthalpy- and temperature profile across a liquid-vapor interface with a continuous description throughout the interfacial region (grey areas).

When the measurable heat flux is determined in the vapor phase, the driving force due to a difference in chemical potential must be evaluated at the temperature of the liquid phase

$$X_{\mu}^{g} = -\frac{1}{T^{l}}\left(\mu^{g}(T^{l}) - \mu^{l}(T^{l})\right), \tag{28}$$

$$= -\left(\frac{\mu^{g}(T^{g})}{T^{g}} - \frac{\mu^{l}(T^{l})}{T^{l}}\right) + h^{g}\left(\frac{1}{T^{g}} - \frac{1}{T^{l}}\right), \tag{29}$$

$$\approx -R_{w}\ln\left(\frac{p^{g}}{p_{\mathrm{sat}}(T^{l})}\right). \tag{30}$$

Eqs. 25, 26, 28 and 29 are exact formulations while Eqs. 27 and 30 represent approximations [29]. We have compared the three formulations of the driving forces for all evaluated experiments and found good agreement. Arguably, the expressions in Eqs. 27 and 30 are the simplest expressions for the chemical driving forces, and are therefore recommended for general use.

2.2.2. Integral relations and square gradient theory

NET treats the whole of the interfacial region (grey areas in Fig. 1) as an autonomous thermodynamic system. Properties of the interface are described as overall excess variables, with respect to the position, ξ, of the Gibbs dividing surface [29]. Once the local description of the heat transfer resistance throughout the interface, r_{qq}, is known, it can be used to determine the interface transfer coefficients by use of the integral relations [38]:

$$R_{ij}(T,\xi) = \int_{-\infty}^{\infty} dz[\phi_{ij}(z)^{\mathrm{ex}}]. \tag{31}$$

Here, z is the direction perpendicular to the interface. The transfer coefficients are excess variables where $\phi_{ij}(z)^{\mathrm{ex}} = \phi(z) - \phi^{\mathrm{left}}\Theta(\xi - z) - \phi^{\mathrm{right}}\Theta(z - \xi)$. Here, superscripts left and right indicate the position on the left- or right hand side of the dividing surface and Θ is the Heaviside function. The integral relations are $\phi_{qq} = r_{qq}$, $\phi_{q\mu} = r_{qq}(h^{\mathrm{pos}} - h)$ and $\phi_{\mu\mu} = r_{qq}(h^{\mathrm{pos}} - h)^2$. Here, h^{pos} is the enthalpy of the adjacent bulk phase and h is the local enthalpy throughout the interface (compare Fig. 1). The enthalpy of the adjacent bulk phase is $h^{\mathrm{pos}} = h^{l}$ when choosing the measurable heat flux on the liquid side, while it is $h^{\mathrm{pos}} = h^{g}$ when choosing the measurable heat flux on the vapor side. The integral relations have been verified to work, e.g. by comparing to simulation results for a Lennard-Jones spline potential [39].

A continuous description of thermodynamic properties throughout the interface can be obtained by square gradient theory (SGT). In SGT, the Helmholtz energy functional contains a contribution from the square of the density gradient [40]:

$$F[\rho(z),T] = \int dz\left[f_{eos}(\rho(z,T) + \frac{1}{2}\kappa(T)|\nabla\rho(z)|^{2}\right], \tag{32}$$

where z is the position perpendicular to the interface, f_{eos} is the Helmholtz energy density given by the EoS, and κ is the influence parameter. The equilibrium density profiles and other thermodynamic variables can be determined through the interfacial region by minimizing the Helmholtz energy at a fixed total number of particles and temperature. This results in a continuous, thermodynamically consistent description of thermodynamic variables through the interface, which depends on temperature, density, and the density gradient. The specific enthalpy is:

$$h_{SGT}(\rho(z),T) = h_{eos}(\rho(z),T) - \frac{T}{2}\frac{\partial\kappa(T)}{\partial T}|\nabla\rho(z)|^{2} - \rho(z)\kappa(T)\nabla^{2}\rho(z), \tag{33}$$

where h_{eos} is the enthalpy given by the EoS. The variables obtained from SGT can be used to determine the local thermal resistivity, which is defined by $r_{qq} = (\lambda T^{2})^{-1}$ for bulk phases.

Table 1
Sets of experiments and notation of the different sets.

Experiment Number	Reference	Set number
1 - 45	Badam et al. [13]	①
46 - 65	Jafari et al. [22]	②
66 - 70	Kazemi et al. [23]	③
71 - 75	Kazemi et al. [24]	④
76 - 149	Kazemi et al. [14] (PMMA)	⑤
150 - 159	Kazemi et al. [14] (Steel)	⑥

2.3. Kinetic theory of gases

Kinetic theory of gases (KTG) was originally derived for simple hard spheres and not for water [41]. Since the pioneering work of Hertz [42] and Knudsen [43], KTG, however, has frequently been used to study water evaporation. The mass flux across the interface from the HK equation is

$$J_{\mathrm{HK}} = \sqrt{\frac{m}{2\pi k_{B}}}\left(\sigma_{e}\frac{p_{\mathrm{sat}}(T^{l})}{\sqrt{T^{l}}} - \sigma_{c}\frac{p^{g}}{\sqrt{T^{g}}}\right), \tag{34}$$

where σ_e and σ_c are the evaporation- and condensation coefficients, respectively. Several formulations of the HK equation exist, with varying assumptions for the two unknown coefficients. An in-depth review of the different formulations of the HK equation was presented by Persad and Ward [30]. A full set of interface relations for heat and mass transfer in NET that is based on KTG is given by Kjelstrup and Bedeaux [29]. These transfer coefficients were derived by Cipolla et al. [28] for hard spheres and are presented and discussed in the supplementary information. We shall in the following focus on a formulation by Schrage [44], who corrected the HK equation to include the bulk velocities of the vapor. Assuming that $\sigma_e = \sigma_c$, the HK-Schrage expression can be written as:

$$J_{\mathrm{HKS}} = \frac{2\sigma_{c}}{2-\sigma_{c}}\sqrt{\frac{m}{2\pi k_{B}}}\left[\frac{p_{\mathrm{sat}}(T^{l})}{\sqrt{T^{l}}} - \frac{p^{g}}{\sqrt{T^{g}}}\right]. \tag{35}$$

We shall further make use of the explicit expressions for the condensation and evaporation coefficients from SRT (see Eq. 15 and 16) for a comparison with those from the HK-Schrage expression.

3. Methodology

This section is divided into four subsections to enhance readability. The three theories have been evaluated by means of 6 data sets containing in total 159 single experiments. An overview of the sets of experiments is summarized in Table 1.

The post-processing procedure of the experimental data from these sets is described in Section 3.1. The fluxes we determine are subsequently used to evaluate the three theories in question. SRT has no unknown coefficients but gives explicit expressions for the evaporation fluxes. The evaluation procedure of these expressions is described in Section 3.2. NET has three unknown coefficients that will be determined from experimental input. The determination of these coefficients and how they are further evaluated by means of the experimental data is described in Section 3.3. KTG has two unknown coefficients. We shall evaluate two expressions from KTG, one assuming equality between the coefficients and one that gives explicit expressions for the coefficients. The evaluation of these expressions is described in Section 3.4.

3.1. Post-processing of the experimental data

The interface of the liquid in the experimental apparatus was held at a constant position during the steady-state evaporation experiments. This was done by carefully regulating the supply of liquid. The supply of liquid gives the overall evaporation rate of the experiment, which

may differ from the local one [22]. The evaporation chamber was evacuated before each experiment, such that water was the only component present in the chamber. The vapor pressure of water could thus be determined by measuring the overall pressure in the vapor phase. For all experiments, also the temperature profiles on both sides of the interface were measured. From these data, we first computed the heat fluxes adjacent to the liquid-vapor phase, i.e. on the liquid- and the vapor sides.

The heat fluxes on the two sides of the interface can be computed from knowledge of the temperature profile and the thermal conductivity of the phase. Temperature profiles and vapor pressures were available for experiment sets 1, 2, 3, and 4. The temperature profiles were either provided to us by the authors or extracted from the published profiles using PlotDigitizer [45]. Sets 5 and 6 did not have this information and we used the heat fluxes given in the publication.

To determine the heat fluxes, we first used a polynomial to fit the temperature profiles in the liquid and the vapor phases. The fitted polynomials were either of first- or second-order, due to the different shapes of the temperature profiles. The measurable heat fluxes were determined in the vapor and liquid phases from Fourier's law using the temperature gradient.

The thermal conductivity was determined using the CoolProp package [46] with local density and temperature as input values. CoolProp uses the state of the art IAPWS formulation for thermodynamic properties of water [47] and an updated version of the IAPWS formulation for the thermal conductivity [48]. The density of the vapor phase was obtained by assuming a constant vapor pressure in the evaporation chamber. We determined the local density from the ideal gas law

$$\rho^g(z) = \frac{p_{exp}}{R_w T^g(z)}, \tag{36}$$

where ρ^g is the density of the vapor, R_w is the specific gas constant of water, and T^g is the local temperature in the vapor phase. The assumption of a constant vapor pressure inside the evaporation chamber is supported by Kazemi and Ward [14]. They showed that the vapor pressure is constant perpendicular to the interface during steady-state evaporation. The density of the liquid was determined by the saturation density at the given temperature of the liquid, which is a good approximation for the low temperature regime:

$$\rho^l = \rho^{l*}(T^l) \tag{37}$$

where ρ^{l*} is the saturation density.

The heat and mass fluxes should be consistent with the mass-, energy- and momentum- balances at the interface. This becomes especially important as the evaporation flux in an experimental set-up may vary along the liquid-vapor interface perpendicular to the transport direction [22]. A consequence of this is that the local evaporation flux can differ from the experimentally determined averaged overall evaporation flux. We have therefore re-analyzed the experimental data by means of the mass-, energy- and momentum- balances, which reduce to a set of constant fluxes at steady-state (see Eqs. 1 - 3). Eqs. 1 - 3 were solved with the heat fluxes, temperatures, and pressures in the vapor phase from experiments as fixed input values. The velocities in the liquid and vapor phase were determined using Eq. 1 and the pressure in the liquid phase by the IAPWS formulation with density and temperature of the liquid as input values. We found the kinetic contributions in the momentum- and energy balances to be sufficiently small (< 0.2%) to be neglected.

The procedure above was used to investigate whether the experimentally determined overall evaporation rate differed from the local. By solving the three balance equations Eqs. 1 - 3, it is possible to find a set of fluxes that are in correspondence with the local heat fluxes, determined via the temperature profiles. We found good agreement between the obtained mass fluxes and the ones measured by Jafari et al.[22] and by Kazemi et al. [23] who used a similar procedure to determine the rate of evaporation. By solving the balance equations in this way, however, certain multidimensional effects have been neglected, which will be discussed further in Section 4.

3.2. Evaluating statistical rate theory

SRT has no unknown coefficients. The evaporation flux can thus be predicted from fluid properties and knowledge of temperatures and pressures. The solutions to SRT were found by solving Eqs. 7 - 10. The key variable in SRT is the deviation of entropy during steady-state evaporation compared to the equilibrium situation. This difference in entropy can either be described by the equations provided by Kazemi and Ward [14] (Eqs. 11 - 13) or by a suitable equation of state (EoS). We have compared the expressions from Eqs. 11 - 12 to the determination of the entropy difference using the state-of-the art IAPWS formulation for water (see supplementary information) and found good agreement between both approaches. For simplicity, we have therefore chosen to use the expressions given in Eqs. 11 - 13. Here, curvature effects were neglected due to their small contributions [24], i.e. $C = 0$ in Eq. 11.

The equations of SRT were found to give results strongly dependent on the pressure in the vapor phase [14]. We, therefore, chose to study the sensitivity of SRT with respect to the pressure difference between the saturation pressure and the actual pressure in the vapor phase. To do this, we refitted the vapor pressure to match the local evaporation rate in SRT. This procedure was also employed by Kazemi and Ward [14]. The vapor pressure was made a free variable within the range -10 Pa $\leq p_{sat}(T^l) - p^g \leq +$ 35 Pa. We decided for this range as it covers the whole range of measured differences between the vapor pressure and the respective saturation pressures, including the uncertainties.

3.3. Determination of coefficients in non-equilibrium thermodynamics

The Onsager relations [36,37] ($R_{q\mu} = R_{\mu q}$) leaves NET with three unknown coefficients to be determined for two force-flux equations. Integral relations have been developed to help in this situation [38] and we have chosen to combine the integral relations with SGT for the determination of the coefficients. Solving SGT profiles requires an EoS. The cubic plus association (CPA) EoS has been used to represent the properties of water. We have refitted the CPA EoS by Queimada et al. [49] to increase the accuracy in the supercooled regime, see the supplementary information. We further used a temperature-dependent influence parameter, $\kappa(T)$, to account for the anomalous behavior of the surface tension of water as a function of temperature [50]. Using SGT together with the integral relations has the advantage that the obtained coefficients are thermodynamically consistent and that the fitting procedure reduces to only one unknown quantity that needs to be determined for each experiment; the local heat transfer resistance, r_{qq}, through the interface [51]. We found that the following expression reproduced most precisely the fluxes from the steady-state evaporation experiments.

$$r_{qq}(z) = \frac{1}{\lambda(T,\rho)T(z)^2} + \left(\frac{\beta_1(T^l)}{\rho(z)^{1.5}} + \frac{\beta_2(T^l)}{\rho(z)^{4.5}}\right)|\nabla\rho(z)|^2, \tag{38}$$

where β_1 and β_2 are parameters that need to be determined. Eq. 38 ensures that the local description of the thermal resistance is always positive through the interfacial region, which gives a strictly positive local entropy production, in-line with the second law of thermodynamics.

We computed the three coefficients, R_{qq}, $R_{q\mu}$ and $R_{\mu\mu}$ for each single experiment using a fitting procedure. The fitting procedure used to determine the coefficients in NET is explained by means of the flow chart in Fig. 2. Each experiment was treated independently from the others, and the gas- and liquid side coefficients were determined for each experiment. The coefficients are known to depend on the temperature of the surface [29,51,52]. The temperature of the surface, T^s, was approximated as the liquid phase temperature, $T^s \simeq T^l$ [26].

We first solved SGT to obtain equilibrium profiles across the interface at temperatures of the liquid-phase. Solving the SGT profiles gives for each experiment a continuous description of the enthalpy, $h(z)$, the density, $\rho(z)$ and the gradient in density $\nabla\rho(z)$ through the interface. We further determined the local thermal conductivity, $\lambda(z)$, using the

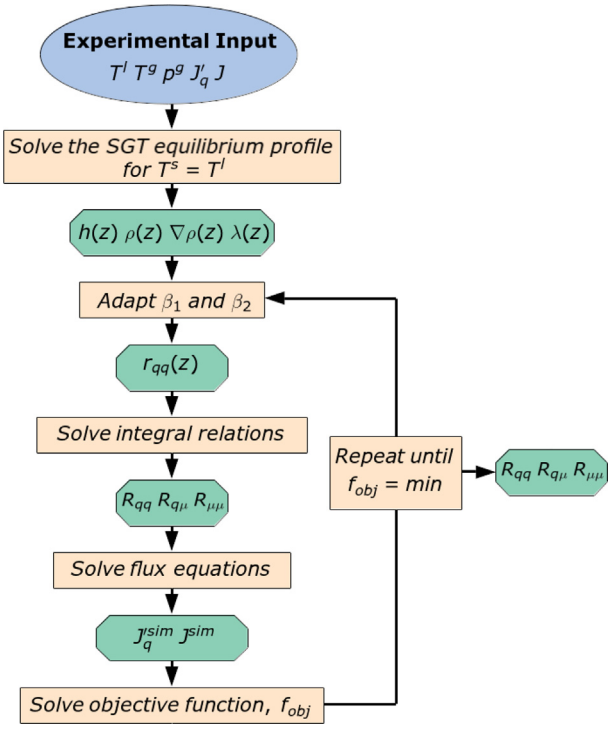

Fig. 2. Flow chart of the fitting procedure used to determine the interface resistances of NET.

CoolProp package with the local density and temperature as input values[46].

The next step was to carry out a minimization procedure. The purpose of the minimization procedure was to find the NET interface coefficients that minimize the difference between the predicted fluxes and the experimental ones. The minimization procedure used the following objective function:

$$f_{obj} = \sqrt{\left(\frac{J'_q - J'^{\text{sim}}_q}{S_Q}\right)^2 + \left(\frac{J - J^{\text{sim}}}{S_J}\right)^2}, \tag{39}$$

where J'_q and J are the measurable heat flux and the mass flux from the steady-state evaporation experiment. The fluxes obtained by inverting the flux equations (see Eqs. 17 and 18) are denoted by superscript sim. The expressions from Eqs. 27 and 30 were used for the determination of chemical driving forces. We used scaling parameters to account for the different order of magnitude of the two fluxes. These were S_Q = 250 J/m^{2}s for the measurable heat flux and $S_J = 10^{-4}$ kg/m^{2}s for the mass flux. The scaling factors were chosen such that they have a typical value of the mass- and heat fluxes and such that the ratio between them was approximately equal to the average evaporation enthalpy in the considered temperature range, $S_Q/S_J \approx \Delta H_{ev} \approx 2.5 \cdot 10^6$ J/kg.

The minimization procedure was performed by adapting β_1 and β_2 from Eq. 38. Knowledge about the local heat transfer resistance, $r_{qq}(z)$, enables the determination of the overall resistances (R_{qq}, $R_{q\mu}$ and $R_{\mu\mu}$) of the liquid-vapor interface by solving the integral relations. The integral relations were solved with the equimolar surface as dividing surface, ξ (see Eq. 31). The overall resistances were then used to determine the measurable heat flux, J'^{sim}_q, and mass flux, J^{sim}, by solving the flux equations with the given experimental temperatures of the liquid and vapor as well as the pressure of the vapor phase. This procedure was performed using both the measurable heat flux on the gas side, J'^g_q, and the one on the liquid side, J'^l_q. The fitting procedure was done with the "fminsearch" function of MATLAB.

The use of a minimization procedure bears the risk of finding local minima. Treating each experiment independently from the others has the advantage that the consistency of each experiment can be assessed using the conversion between the gas and liquid side (see Eqs. (19 - 23). It further enables us to inspect whether the regressed coefficients follow reasonable trends with respect to the temperature of the surface without a priori imposing any assumptions. Also, the risk of local minima can be decreased by varying the starting values for β_1 and β_2 in a wide range for each experiment. The procedure allowed us to determine a consistent set of gas- and liquid-side coefficients. The presented procedure has two drawbacks. First, it gives β_1 and β_2 the possibility to fluctuate and vary from experiment to experiment. This means that β_1 and β_2 cannot be used for extrapolation to other temperature regimes. Next, by using the experimentally determined values we may induce a bias on the coefficients, originating from systematic or unsystematic uncertainties in the experimental data.

The computed NET coefficients were found to be very sensitive to the pressure of the vapor phase and the temperature jump. Only data sets 1, 5, and 6 provided large enough fluxes and temperature jumps to allow coefficients determination within the same order of magnitude. Coefficients from sets 2, 3, and 4 varied by two orders of magnitudes. We, therefore, show only coefficients from sets 1, 5, and 6 in the results sections and discuss their thermodynamic consistency and trends with respect to the temperature of the liquid. Based on this discussion, we have chosen the most meaningful ones and present them as average coefficients, with a linear variation in the temperature regime of the experiments. These linear fits of the coefficients are next used to reproduce the fluxes from all experimental sets (1–6). In Section 5, we first evaluate these fits using the experimental values as input. Next, we will make the vapor pressure a free variable in order to study the sensitivity of the results with respect to the vapor pressure by matching the experimental fluxes. The pressures used are in the range -10 Pa $\leq p_{sat}(T^l) - p^g \leq +$ 35 Pa.

3.4. Evaluating kinetic theory of gases

KTG has two unknown coefficients, which are the evaporation- and the condensation coefficient [30]. We have evaluated the HK-Schrage expression by assuming equality between the evaporation- and condensation coefficient (see (Eq. 35)). The condensation coefficients for the HK-Schrage equation were obtained by matching the mass flux. The obtained condensation coefficients are compared with the explicit expressions from Persad and Ward that are based on SRT (see Eqs. 15 and 16).

4. Preliminary evaluation of experiments

We start with a discussion of the experiments and their uncertainties. In order to obtain an overview of the experimental results, we have shown the result for each variable as a function of the experiment number in Figs. 3 and 4. In all experiments, the temperature of the liquid adjacent to the interface was in the range of 258 K - 281 K. The temperature of the liquid determines the equilibrium saturation pressure which was in the range of 200 Pa - 1062 Pa. For set 1, a heating element in the vapor phase was used to induce larger heat fluxes to the interfaces from the vapor side. Sets 2 - 6 used a heat exchanger on the liquid side to control the temperature of the liquid.

The difference between the saturation pressure and the actual pressure of the vapor phase is shown in Fig. 3 a). A significant scatter is seen in the data. Relatively large pressure differences were determined in the experiments from sets 1 and 6, while the pressure differences from sets 2 - 5 exhibited a fluctuating behavior around the saturation pressure. The temperature jumps and their uncertainties are shown in Fig. 3 b). The magnitude of the temperature jumps varies significantly. While it is possible to identify clear temperature jumps for sets 1, 5, and 6, the temperature jumps of sets 2–4 are so close to zero that they fluctuate between positive and negative values within the reported uncertainty.

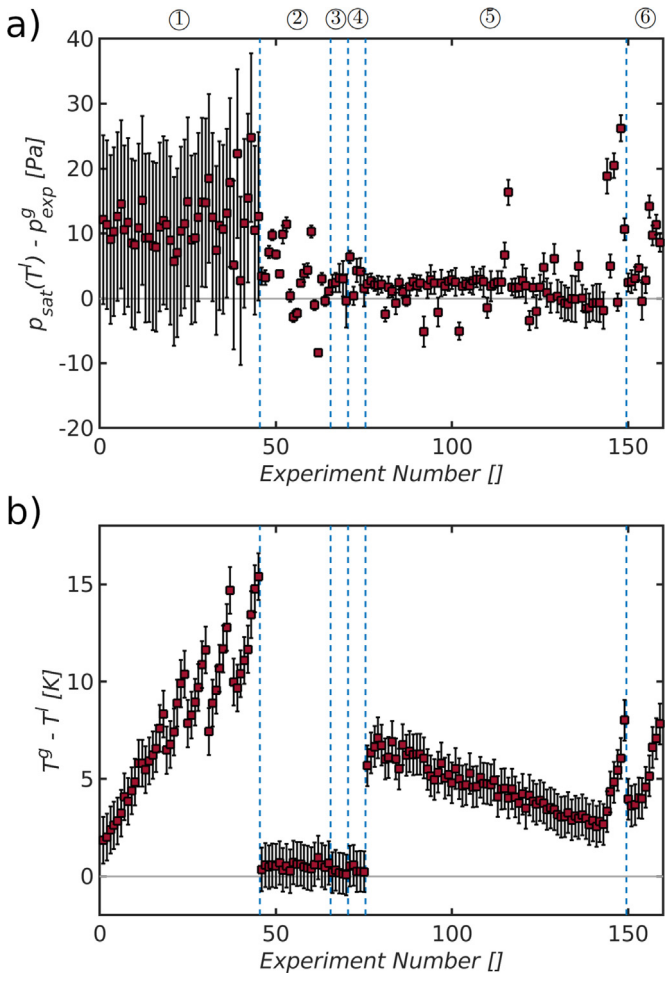

Fig. 3. Comparison between the experimentally determined values of the different data sets for a) the difference between saturation pressure and the experimentally determined vapor pressure and b) the observed temperature difference between vapor and liquid phase.

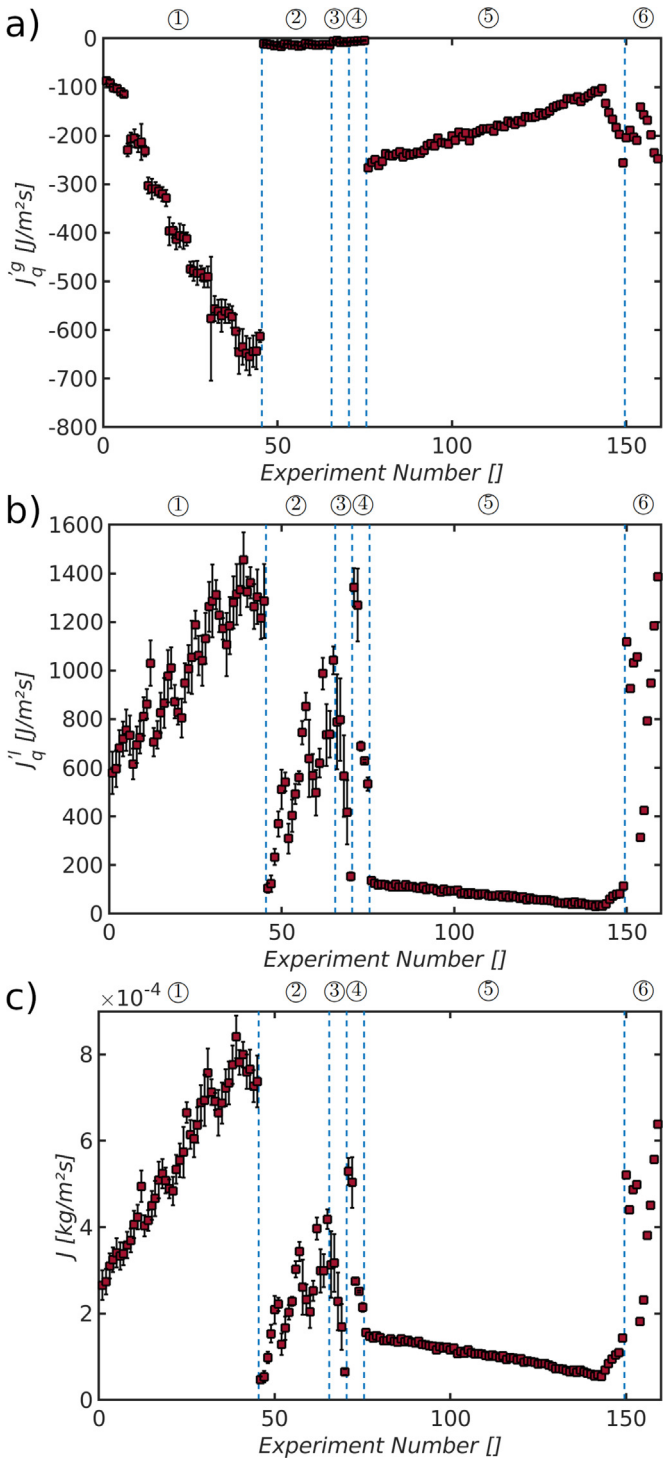

Fig. 4. Comparison between the experimentally determined values of the different data sets for a) the measurable heat fluxes on the gas side b) the measurable heat fluxes on the liquid side and c) the evaporation mass fluxes.

The measured temperature jumps are more affected by the heat flux on the vapor side (Fig. 4 a) than by the one on the liquid side (Fig. 4 b).

This is particularly clear when we consider sets 2–4, where the temperature jumps remain within the range 0.14 K - 0.55 K, despite large liquid side heat fluxes. A direct connection between the vapor side heat flux and the temperature jumps was also pointed out by Badam et al. [13] and is further supported by Wilhelmsen et al. [51] with results for Lennard-Jones fluids. There, the main resistance to heat transport appeared on the vapor side of the interface. While it is possible to identify a relation between the temperature jump and the measurable heat flux on the vapor side, the connection between the pressure difference and the fluxes is less clear. The uncertainties and fluctuating behavior of the experimentally determined vapor phase pressures are too large to make any conclusion about any trends on this topic.

As explained in the Methodology Section, the heat and mass fluxes (Fig. 4 c) are computed from the temperature profiles adjacent to the interface, assuming that the system can be described as an effective, one-dimensional transport process. The liquid side heat flux is the dominant energy supply to the interface for most of the sets. The vapor side heat fluxes are only larger than the liquid side ones for set 5. Since the mass fluxes were determined by solving the energy balance (see Eq. 3), they follow the trends of the liquid side heat fluxes of sets 1, 2, 3, 4, and 6. The uncertainties shown in the figures include experimental uncertainties in the temperature measurement as well as uncertainties derived from the polynomial fit to the temperature profiles. The uncertainties were determined, using Gauss' law of error propagation. Fluxes from sets 5 and 6 are shown without statistical uncertainties. An evaluation of systematic measurement errors is much more difficult. This issue becomes especially relevant as it was shown that the measured temperature jumps can depend on the chosen thermocouple [14] and may also be influenced by heat conduction in the thermocouple, inaccessibility of the interface or rarefaction effects [27]. Here, it is especially the vapor-

phase temperature that is prone to systematic measurement errors [27]. We have not been able to account for them in the present study.

Another possible source of error is the simplification to a one-dimensional transport problem. It was shown that complex flow patterns in the liquid and the vapor phase can evolve during evaporation experiments [23]. They can occur due to buoyancy effects, thermocapillary flow along the surface, Marangoni effects, or disturbances by the presence of the thermocouple [27,53–55]. Three-dimensional heat conduction effects from the sides of the evaporation container may also be present. Heat conduction from the sides impacts especially the liquid side heat flux, which can be seen by comparing sets 5 and 6. While the experimental set-up was the same for both sets, the evaporation container was made out of PMMA in set 5 and the one of set 6 consisted of stainless steel [14]. The thermal conductivity of the container materials in the experiments affects the heat conducted horizontally to the interface. An indication of the presence of such effects is non-linear temperature profiles and a two-dimensional numerical model may therefore be needed for a priori prediction of these temperature profiles [23]. In the present study, we used the experimentally determined one-dimensional temperature profiles. These profiles already include local effects and we have assumed that the heat transfer via conduction is described by Fourier's law sufficiently close to the interface. The validity of this assumption is supported by the good agreement of the obtained evaporation fluxes and the ones from Kazemi et al. [23] who used a two-dimensional model for the determination of the evaporation fluxes. The chosen approach of determining the local fluxes is not only common practice in the literature [14,22], but was also necessary due to lack of knowledge of the exact conditions at the inlet and outlet as well as of the surrounding of the evaporation container for some of the sets. The experimental data discussed above shall now be used to evaluate the three theories in question.

5. Results and discussion

In the following, we examine the three theories in question and discuss whether they give a good representation of the experimental data presented in Section 4. A discussion follows, including how to obtain more experimental results that can further enhance the understanding of evaporation. This follows in Section 5.4.

5.1. Statistical rate theory

As discussed in the Methodology section, the expressions of the mass flux from SRT were evaluated using the entropy difference between the liquid and vapor states at the interface. The evaporation flux computed from SRT in this way (Fig. 5 a) does not show any reasonable agreement with the experimental value of the mass flux. The predicted values deviated from the experimental values by up to two orders of magnitude. The scatter in the predicted evaporation flux mirrors the scatter in the pressure difference, which can be seen by comparing to Fig. 3 a). The predictions from SRT are clearly most sensitive to the deviation of the pressure in the vapor phase from the saturation pressure.

The sensitivity of SRT to the pressure difference is of interest. The vapor pressure was therefore refitted to match the measured evaporation flux. The vapor pressure difference so obtained is compared to the experimentally determined one in Fig. 5 b).

The large sensitivity of the mass flux towards the vapor pressure enables us to fit the evaporation flux within a small range away from the saturation pressure. It was possible to match most of the evaporation fluxes with a pressure difference of only 1 Pa. The largest pressure difference needed to match the respective evaporation flux was 3 Pa. However, this result does not agree with the measured pressure differences. Here, set 1 is particularly notable. Shifting the pressure difference from around 10 Pa to 1–3 Pa changes the predicted evaporation flux by two orders of magnitude. The pressure difference obtained follows the expected trend, i.e. the larger the pressure difference, the larger the evaporation flux.

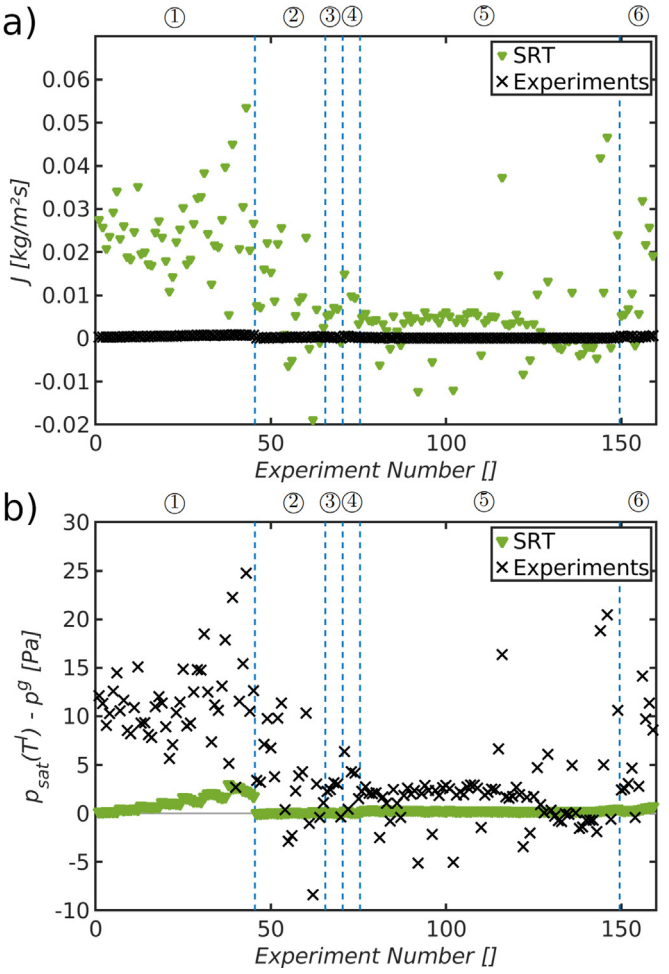

Fig. 5. a) The predicted and experimental evaporation flux from SRT and b) the pressure difference obtained from SRT after fitting the vapor phase pressure to match the experimental evaporation flux.

SRT appears to under-predict the experimental pressure difference in most of the experiments. The predicted pressure difference is, however, for many of the experiments within the statistical error of the experiments. The uncertainty in the experimentally determined vapor pressure is large (see Fig. 3 a). An exception is data set 6, where the vapor pressure differences are larger and show a systematic trend with relatively small uncertainties. A conclusion on whether the predictions from SRT agree or not with experimental data is not possible because there are too few data points available with small uncertainties and significant pressure differences.

5.2. Non-equilibrium thermodynamics

We shall next evaluate the NET expressions for interface transfer of mass and heat. We start with a presentation of the NET coefficients obtained from the integral relations and SGT. An evaluation follows of the NET coefficients concerning to their ability to reproduce the experimentally determined fluxes.

The coefficients from NET will be evaluated by their overall trends, magnitudes, and by consistency checks. All coefficients were found to be consistent with respect to the conversion from the liquid- to the gas side and vice versa (compare Eqs. 19–23). The coefficients were also found to obey the criterion set by a positive entropy production [29], which means that the product of the main coefficients must be larger

than the one of the coupling coefficients ($R_{qq}R_{\mu\mu} - R_{q\mu}R_{q\mu} > 0$). Lastly, the liquid side coupling coefficients were found to be negative while the vapor side coefficients were found to be positive. This is in agreement with the criterion set by the integral relations.

While all coefficients were found to fulfill these consistency checks, they did not show a clear trend with respect to the temperature of the liquid-phase, where $T^s \simeq T^l$. Data sets 1 and 6 appeared to follow the same trend, however, and have similar magnitudes, while data set 5 deviated clearly from the two other data sets. The difference between the data sets is especially clear when we examine the gas-side coefficients. The difference between the liquid- and gas side coefficients is notable. We further observed that the coefficients of set 5 increased with increasing temperature of the liquid, while the coefficients from sets 1 and 6 exhibited the opposite behavior. This points toward an inconsistency in data set 5, since it is known that the coefficients should decrease with increasing temperature of the surface [29,51,52]. The opposite trend of data set 5 stems from a larger deviation with respect to the other sets for temperatures above 270 K. A personal communication with Kazemi [14] revealed that one of the pressure transducers was customized to the pressure range 0 - 500 Pa. For data set 5, the experimentally determined pressures below 500 Pa should thus be the most accurate, which could explain a stronger deviation from the other coefficients above 270 K. Another explanation may be provided by the absolute value of the pressure differences of the experiments. While the measured vapor pressures of sets 1 and 6 are clearly below the respective saturation pressure, the ones from set 5 are closer to the saturation pressure. The relative change of the chemical driving force of set 5 was thus much more sensitive to the experimental uncertainties compared to those from sets 1 and 6. Systematic errors in the temperature measurements may be another reason for the deviations between the coefficients. The problem of systematic errors was discussed by Kazemi and Ward [14], who showed that the measured temperatures of the gas phase from data set 5 depended on the wire thickness of the thermostat.

We found that the coefficients from data set 1 also depended on the experimental set-up, which is indicated by the two different shades of blue in the figure. A heating device located above the liquid-vapor interface in data set 1 was used to induce larger vapor side heat fluxes [13]. The heating device was either turned off (NH) or turned on (H). The deviating coefficients observed for these two conditions may indicate a systematic measurement error. The coefficients in NET should for a single-component system only depend on the properties of the surface, and not on the experimental conditions. This means that the coefficients should not depend on whether the heater is turned on or not. A similar supposition about experiment set 1 was made by Kazemi et al. [27] who found in a numerical study that the heater may have influenced the temperature measurement in the gas phase. We have highlighted these discrepancies in the different data sets. The constraints imposed by the framework of SGT enabled us to identify these deviating behaviors. SGT is therefore not only a useful tool to deal with uncertainties but also to identify deviating or thermodynamically inconsistent behaviors. This means that for the given data sets, we were unable to determine a uniform set of coefficients, but only to give an order of magnitude estimate of the coefficients. We further compared the total magnitude of the coefficients to the ones predicted by KTG [29] (see supplementary information). Here, we found the coefficients from KTG to be one to two orders of magnitude smaller than the ones presented in Fig. 6. A larger deviation, however, is not surprising since the coefficients from KTG were derived for hard spheres and not for water.

Due to the deviating behavior of the coefficients from data set 5 with respect to the temperature of the liquid phase, we will in the following exclude this data set for the approximation of the coefficients. The coefficients will be analyzed by linear fits of sets 1 and 6 in the given temperature regime. The fit was done with respect to the temperature of the liquid and is indicated by the black dashed lines in Figs. 6. The coefficients of these linear fits are provided in Appendix A. The NET coefficients will in the following be evaluated by these linear fits by inversion of the force-flux equations (Eqs. 17 and 18) to predict the fluxes at given experimental conditions.

Fig. 7 shows the predictions from NET when using the experimentally determined temperature jumps, vapor pressures, and coefficients at the respective temperatures of the liquid, approximated by the linear fits, as input. The coefficients predict the fluxes from set 1 and set 6 to a reasonable accuracy. Even though the data from the other data sets are not reproduced qualitatively, the right order of magnitude is obtained for the measurable heat fluxes on the vapor side for all sets. The evaporation fluxes and the measurable heat fluxes on the liquid side deviate for sets 2–5. The deviations from data set 2 are notable. While the coefficients from NET appear to predict the first 6 experiments of set 2 with sufficient accuracy, the predicted fluxes deviate clearly for the other experiments. The evaporation chamber of data set 2 was mounted on a heating device to control the liquid side heat fluxes [22]. Similar to set 1, this heater was turned off for the first 6 experiments. This indicates, that the heater may have impacted the determination of the experimental values also in set 2. Also, the constant offset between the predicted evaporation fluxes and the experimental values from data set 5 is noticeable. Here, the predicted evaporation fluxes were approximately two times larger than the experimental values for most of the experiments. The deviations of the predicted measurable heat fluxes on the liquid side are more significant.

While the predictions from NET were deviating for some of the sets, they predicted the right order of magnitude for most of the evaporation fluxes and vapor side measurable heat fluxes. The determined coefficients may thus be used for a rough approximation of the importance of including the interface resistance in models for the description of evaporation- and condensation fluxes in the given temperature regime. By using a sensitivity analysis, we found the evaporation fluxes and the measurable heat fluxes on the liquid side to be more sensitive to the difference between the saturation- and the vapor pressure, while the measurable heat fluxes on the vapor side are more sensitive toward the temperature jumps.

To study the sensitivity of NET with respect to the pressure difference, we refitted the vapor pressure to match the measured fluxes. Fig. 8 shows the resulting predictions. A comparison of Figs. 8 and 7 reveals that a significantly improved agreement with experimental data is possible by small adjustments to the vapor pressure. The measurable heat flux on the vapor side only varied slightly with a change in vapor pressure for sets 2–4, where the temperature jumps remained in a range of 0.14 K and 0.55 K. This again indicates a high sensitivity of the measurable heat flux on the vapor side towards the temperature jump. For the given regime, the measurable heat flux on the vapor side only changes with a change in vapor pressure if the temperature jump is very small. It was possible to obtain good agreement between the predicted and experimentally determined fluxes, due to the sensitivity of the evaporation flux and the liquid side measurable heat flux towards the vapor pressure. Comparing the experimentally determined vapor pressure differences and those obtained from the fit (Fig. 8 d) shows varying tendencies for the different sets. While the fit predicts larger pressure differences for sets 2–4, the pressure of the vapor phase was shifted towards values larger than the saturation pressure for set 5. Considering set 5, two things are particularly noteworthy. First, it is possible to obtain a good match for most of the fluxes by shifting the vapor pressure only 5 Pa, which demonstrates the large sensitivity of the coefficients with respect to the vapor pressure difference. Second, the fitted pressure difference follows the same trend as that from the experiments, which could indicate a systematic error in the measurements used for the determination of the coefficients or in data set 5.

5.3. Kinetic theory of gases

The expressions from KTG were evaluated by fitting evaporation- and condensation coefficients to match the evaporation flux from the

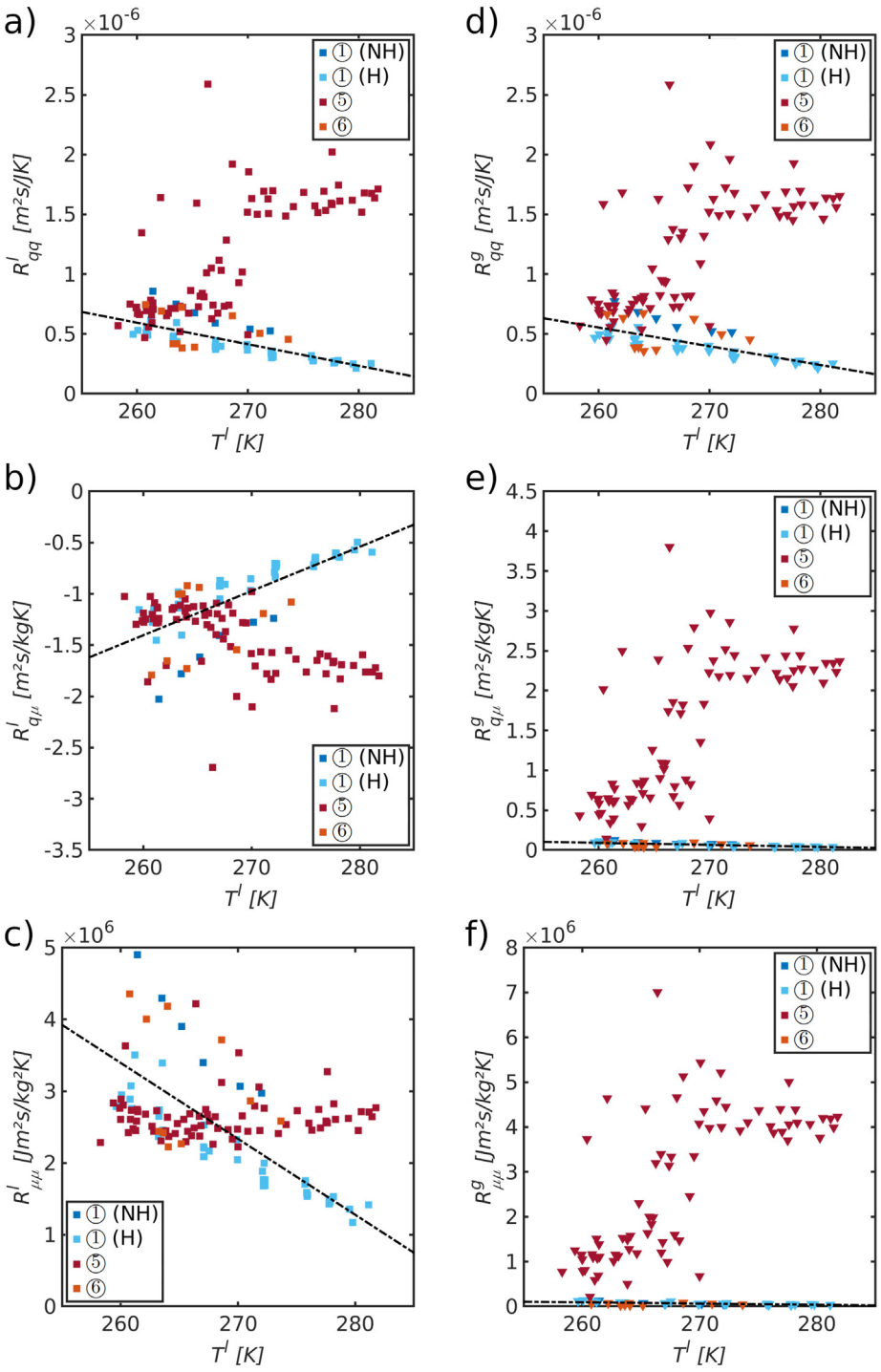

Fig. 6. Transfer coefficients determined using experimental data set 1, 5 and 6. The figures show from top to bottom the resistance to heat transfer, the coupling coefficient and the resistance to mass transfer, respectively. The left column are the liquid-side coefficients and the right column are the vapor-side coefficients.

respective experiments. The coefficients were either obtained by matching the evaporation flux (HKS) or explicitly given (PW), as described in Section 3.4. The condensation coefficients from all experimental sets are shown in Fig. 9. The coefficients span more than two orders of magnitude, a result well-known in the literature[30]. While the coefficients from Persad and Ward [30] are close to unity, the coefficients from the other formulation are two orders of magnitude smaller. We find that the coefficients from the HKS expression from data sets 1 and 5 have the same order of magnitude. The coefficients from data set 5 show a clear decreasing trend with increasing temperature for temperatures below 270 K. A decreasing trend with increasing temperature has also been documented in the literature [56,57]. Similar to the cases of SRT and NET, we found these coefficients to be very sensitive to the vapor pressure.

The explicit expressions for the condensation and evaporation coefficients of Persad and Ward were obtained by neglecting the vibrational contributions of the full SRT expressions [30]. We found the vibrational contribution of the full SRT expressions to be negligibly small for the given data sets (see the supplementary information). Using the explicit expressions for the evaporation- and condensation coefficients results therefore in the same prediction of the evaporation flux as the full SRT expressions (see Fig. 5 a). The prediction captures the difference in magnitude between the different data sets, corresponding to the different pressure differences, but the predictions deviate from the ex-

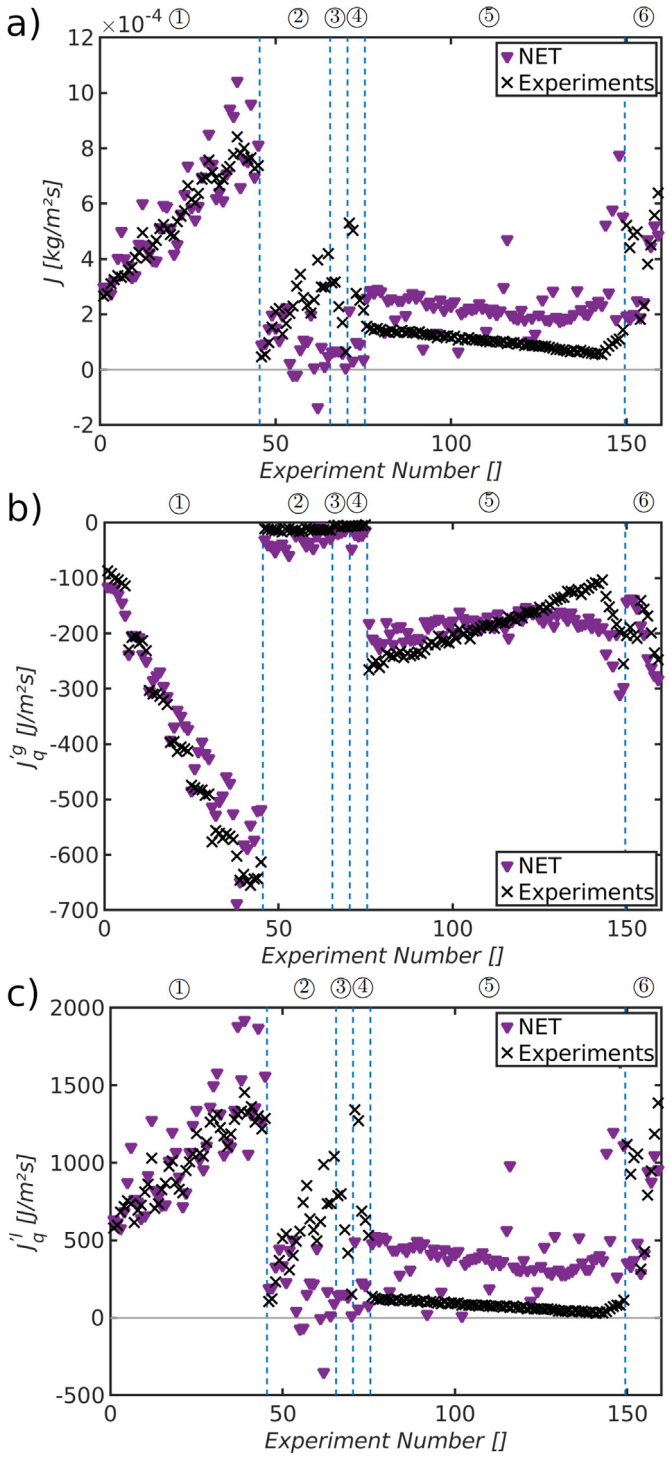

Fig. 7. Comparison of the obtained a) mass fluxes b) measurable heat fluxes on the liquid side and c) measurable heat fluxes on the vapor side with the experimentally obtained values using the different set of coefficients. Here, the experimentally determined pressures were used.

perimental values by several orders of magnitude. The predicted evaporation flux is equally sensitive towards the vapor pressure as the full SRT expressions since the evaporation and condensation coefficients in Eqs. 15 and 16 were obtained from Eq. 7 after the introduction of simplifying assumptions [30]. This may account for the deviating behavior. The condensation coefficients from the HKS-expression are too scattered

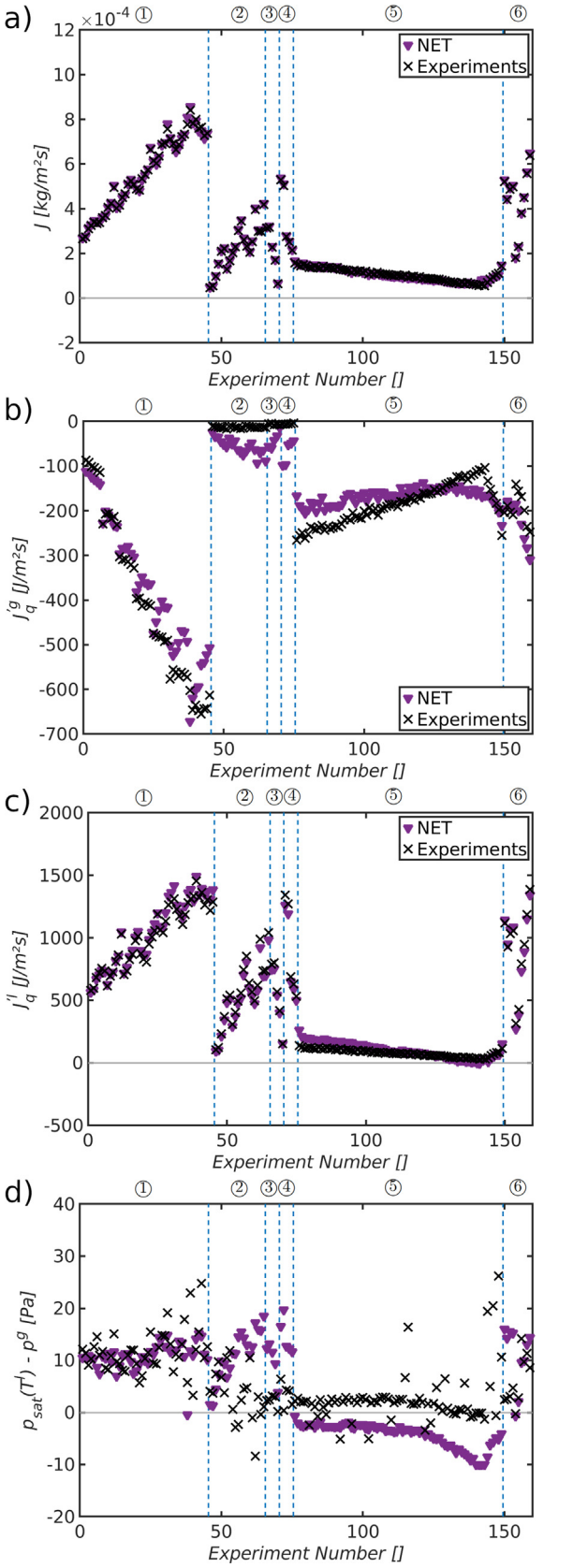

Fig. 8. Comparison of the obtained a) mass fluxes b) measurable heat fluxes on the liquid side and c) measurable heat fluxes on the vapor side with the experimentally obtained values using the different set of coefficients. The difference between the saturation pressure and fitted vapor pressure is compared to experimental values in d).

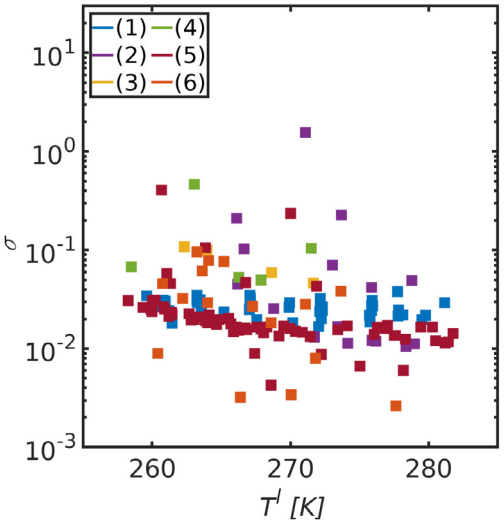

Fig. 9. Condensation coefficients of different KTG formulations as given from (PW) or matched (HKS).

to give physical insights. We conclude that neither of the expressions can predict the mass flux with sufficient accuracy.

5.4. Discussion and guidelines for future experiments

Each theory was described and discussed above. In the following, we present a final comparison and use the insight gained to suggest how future experiments can be carried out.

In the present examination of recently published experiments on evaporation of water, we have found that only NET predicted the right orders of magnitude of the evaporation fluxes, after determination of the coefficients. The evaporation fluxes predicted by SRT deviated up to two order of magnitude from experiments, and also the condensation coefficients of KTG were varying by two orders of magnitude. The predictions from all three theories are, however, very sensitive to the conditions at the liquid-vapor interface, in particular, the vapor pressure during evaporation. While it was possible to determine coefficients from NET, we found during the determination and evaluation of the coefficients indications of systematic measurement errors in some of the data sets. Due to these indications and large uncertainties in the measurements of the vapor pressure, it is thus not possible to give a conclusive evaluation of the ability of the three theories to describe steady-state evaporation experiments of water in the considered temperature regime.

To increase the accuracy of the NET coefficients and to evaluate the three theories with a higher degree of confidence, future experimental works should focus on measuring vapor pressures with higher accuracy (<0.3 Pa). We have seen that a difference of a few Pascal only, can significantly change the predicted evaporation fluxes in NET and SRT, and the condensation coefficients from KTG. Here, the use of multiple pressure transducer, as performed by Kazemi and Ward [14], is likely to reduce the uncertainty.

Particular attention should also be devoted to avoiding systematic measurement errors. Here, it is especially the influence of the heating device on the temperature measurement in the vapor phase that must be considered. While the impact of heating devices on the measured vapor phase temperature has been discussed before [27], we found that also mounting the evaporation chamber on a heat exchanger may impact the experimental values. This finding should be considered and investigated further in future evaporation experiments. Thermodynamic consistency checks are useful to identify systematic measurement errors, as shown in this work for the evaluation of the coefficients from NET (see Section 5.2).

Also, a wider range of fluxes, temperature jumps, and temperatures of the liquid could be used, to increase the accuracy of the coefficients from NET and for a conclusive evaluation of the three theories in question.

While it was possible to identify a direct connection between the temperature jumps and the measurable heat fluxes on the vapor side, the connection between the fluxes and the pressure difference of vapor pressure and the respective saturation pressure was less clear. Experiments with larger differences between the saturation pressure and the vapor pressure can be helpful to determine this relationship. We found the measurable heat flux on the liquid side predicted from NET to show a larger sensitivity towards the vapor pressure than the measurable heat flux on the vapor side. This connection may be tested by using a larger variation of the liquid side heat fluxes and determination of the vapor pressure. Varying the fluxes in a wider range, however, may cause side effects and complex flow patterns may evolve. A full analysis using a three-dimensional numerical model may therefore be needed to determine the exact fluxes and conditions at the interface.

6. Conclusions

We have presented a critical assessment of six recent experiment sets that report temperature jumps, vapor pressures, and evaporation rates during steady-state evaporation of water. The experiments have been used to evaluate three state-of-the-art theories that take the resistance of the liquid-vapor interface into account; statistical rate theory, non-equilibrium thermodynamics, and kinetic theory of gases.

We found the expressions from statistical rate theory to agree well with the state-of-the-art IAPWS formulation of water for the determination of the entropy difference. However, the comparison to experiments indicates that statistical rate theory under-predicts the difference between the saturation pressure and the actual pressure in the vapor phase. We determined a set of transfer coefficients for the interfacial force-flux relations of non-equilibrium thermodynamics based on the two most consistent data sets. These coefficients predict the right order of magnitude of the evaporation fluxes from the different data sets. During the determination and evaluation of these coefficients, we found indications of systematic measurement errors in some of the data sets. The condensation coefficients from kinetic theory of gases showed a strong sensitivity towards the difference between the vapor pressure and the saturation pressure, similar to the two other theories. The results from kinetic theory of gases were too scattered to provide new physical insight.

All three theories were found to be highly sensitive to the difference between the pressure in the vapor phase and the saturation pressure, resulting in significant variations within a range of only a few Pascals. Even with the increased accuracy of the experimentally determined pressures from a recent study from Kazemi and Ward [14] it was not possible to give a conclusive statement on the feasibility of the theories. More experiments, where the pressure is measured to higher accuracy (<0.3 Pa), would therefore be beneficial for further progress on the important topic of steady-state evaporation of water.

Declaration of competing interest

The authors declare that they have no known competing financial interests or personal relationships that could have appeared to influence the work reported in this paper.

Data availability

Data will be made available on request.

Acknowledgments

The authors greatly appreciate good discussions with Amin Kazemi. We further acknowledge funding from the Research Council of Norway, the Center of Excellence Funding Scheme, Project No. 262644, PoreLab.

Appendix A

The linear fits from Fig. 6 were obtained by fitting the NET transfer coefficients of data set 1 and 6 as a function of the temperature of the liquid.

$$\Omega = a_1 T^l + a_2 \tag{A.1}$$

The coefficients a_1 and a_2 are given in Table A.2 for the respective transfer coefficients.

Table A1
Fitted parameters for the NET transfer coefficients as a function of the temperature of the liquid.

Ω	a_1	a_2
R^l_{qq}	-1.8006e-08	5.2756e-06
$R^l_{q\mu}$	0.0432	-12.6357
$R^l_{\mu\mu}$	-1.0589e05	3.0927e07
R^s_{qq}	-1.5636e-08	4.6189e-06
$R^s_{q\mu}$	-0.0025	0.7415
$R^s_{\mu\mu}$	-2.7399e03	8.0423e05

Supplementary material

Supplementary material associated with this article can be found, in the online version, at doi:10.1016/j.ctta.2022.100091

References

[1] A. Laîné, H. Nakamura, K. Nishii, T. Miyasaka, A diagnostic study of future evaporation changes projected in CMIP5 climate models, Clim. Dyn. 42 (9) (2014) 2745–2761.
[2] S. Al-Obaidani, E. Curcio, F. Macedonio, G. Di Profio, H. Al-Hinai, E. Drioli, Potential of membrane distillation in seawater desalination: thermal efficiency, sensitivity study and cost estimation, J. Membr. Sci. 323 (1) (2008) 85–98.
[3] J. Garatuza-Payan, W.J. Shuttleworth, D. Encinas, D.D. McNeil, J.B. Stewart, H. DeBruin, C. Watts, Measurement and modelling evaporation for irrigated crops in north-west mexico, Hydrol. Process. 12 (9) (1998) 1397–1418.
[4] M. Jonsson, J. Yan, Humidified gas turbines - a review of proposed and implemented cycles, Energy 30 (7) (2005) 1013–1078.
[5] A. Ladha-Sabur, S. Bakalis, P.J. Fryer, E. Lopez-Quiroga, Mapping energy consumption in food manufacturing, Trends Food Sci. Technol. 86 (2019) 270–280.
[6] T. Tanuma, Advances in steam turbines for modern power plants, Woodhead Publishing, 2017.
[7] M.T. Rauter, S.K. Schnell, B. Hafskjold, S. Kjelstrup, Thermo-osmotic pressure and resistance to mass transport in a vapor-gap membrane, Phys. Chem. Chem. Phys. 23 (23) (2021a) 12988–13000.
[8] M.T. Rauter, S.K. Schnell, S. Kjelstrup, Cassie–baxter and wenzel states and the effect of interfaces on transport properties across membranes, J. Phys. Chem. B 125 (46) (2021b) 12730–12740.
[9] M. Maria Antony Raj, K. Kalidasa Murugavel, T. Rajaseenivasan, K. Srithar, A review on flash evaporation desalination, Desalin. Water Treat. 57 (29) (2016) 13462–13471.
[10] S. Hardt, F. Wondra, Evaporation model for interfacial flows based on a continuum-field representation of the source terms, J. Comput. Phys. 227 (11) (2008) 5871–5895.
[11] I. Hitsov, T. Maere, K. De Sitter, C. Dotremont, I. Nopens, Modelling approaches in membrane distillation: a critical review, Sep. Purif. Technol. 142 (2015) 48–64.
[12] F. Duan, C.A. Ward, V.K. Badam, F. Durst, Role of molecular phonons and interfacial-temperature discontinuities in water evaporation, Phys. Rev. E 78 (4) (2008) 041130.
[13] V.K. Badam, V. Kumar, F. Durst, K. Danov, Experimental and theoretical investigations on interfacial temperature jumps during evaporation, Exp. Therm. Fluid Sci. 32 (1) (2007) 276–292.
[14] M.A. Kazemi, C.A. Ward, Assessment of the statistical rate theory expression for evaporation mass flux, Int. J. Heat Mass Transf. 179 (2021) 121709.
[15] D. Kingston, Ø. Wilhelmsen, S. Kjelstrup, The influence of interfacial transfer and film coupling in the modeling of distillation columns to separate nitrogen and oxygen mixtures, Chem. Eng. Sci.: X. 8 (2020) 100076.
[16] L.V. Van der Ham, R. Bock, S. Kjelstrup, Modelling the coupled transfer of mass and thermal energy in the vapour–liquid region of a nitrogen–oxygen mixture, Chem. Eng. Sci. 65 (6) (2010) 2236–2248.
[17] L. Keulen, L.V. Van Der Ham, N. Kuipers, J.H. Hanemaaijer, T. Vlugt, S. Kjelstrup, Membrane distillation against a pressure difference, J. Membr. Sci. 524 (2017) 151–162.
[18] Ø. Wilhelmsen, D. Bedeaux, S. Kjelstrup, Heat and mass transfer through interfaces of nanosized bubbles/droplets: the influence of interface curvature, PCCP 16 (22) (2014) 10573–10586.
[19] Ø. Wilhelmsen, T.T. Trinh, S. Kjelstrup, T.S. van Erp, D. Bedeaux, Heat and mass transfer across interfaces in complex nanogeometries, Phys. Rev. Lett. 114 (6) (2015) 065901.
[20] C.A. Ward, G. Fang, Expression for predicting liquid evaporation flux: statistical rate theory approach, Phys. Rev. E 59 (1) (1999) 429.
[21] G. Fang, C.A. Ward, Temperature measured close to the interface of an evaporating liquid, Phys. Rev. E 59 (1) (1999) 417.
[22] P. Jafari, A. Masoudi, P. Irajizad, M. Nazari, V. Kashyap, B. Eslami, H. Ghasemi, Evaporation mass flux: a predictive model and experiments, Langmuir 34 (39) (2018) 11676–11684.
[23] M.A. Kazemi, D.S. Nobes, J.A.W. Elliott, Experimental and numerical study of the evaporation of water at low pressures, Langmuir 33 (18) (2017) 4578–4591.
[24] M.A. Kazemi, D.S. Nobes, J.A.W. Elliott, Investigation of the phenomena occurring near the liquid–vapor interface during evaporation of water at low pressures, Phys. Rev. Fluids 3 (12) (2018) 124001.
[25] P. Gallo, J. Bachler, L.E. Bove, R. Böhmer, G. Camisasca, L.E. Coronas, H.R. Corti, I. de Almeida Ribeiro, M. de Koning, G. Franzese, et al., Advances in the study of supercooled water, Eur. Phys. J. E 44 (11) (2021) 1–36.
[26] Ø. Wilhelmsen, T.T. Trinh, A. Lervik, V.K. Badam, S. Kjelstrup, D. Bedeaux, Coherent description of transport across the water interface: from nanodroplets to climate models, Phys. Rev. E 93 (3) (2016) 032801.
[27] M.A. Kazemi, D.S. Nobes, J.A.W. Elliott, Effect of the thermocouple on measuring the temperature discontinuity at a liquid–vapor interface, Langmuir 33 (28) (2017) 7169–7180.
[28] J.W. Cipolla Jr, H. Lang, S.K. Loyalka, Kinetic theory of condensation and evaporation. II, Chem. Phys. 61 (1) (1974) 69–77.
[29] S. Kjelstrup, D. Bedeaux, Non-equilibrium thermodynamics of heterogeneous systems, World Scientific, 2008.
[30] A.H. Persad, C.A. Ward, Expressions for the evaporation and condensation coefficients in the hertz-knudsen relation, Chem. Rev. 116 (14) (2016) 7727–7767.
[31] R. Marek, J. Straub, Analysis of the evaporation coefficient and the condensation coefficient of water, Int. J. Heat Mass Transf. 44 (1) (2001) 39–53.
[32] J. Barrett, C. Clement, Kinetic evaporation and condensation rates and their coefficients, J. Colloid Interface Sci. 150 (2) (1992) 352–364.
[33] M. Bond, H. Struchtrup, Mean evaporation and condensation coefficients based on energy dependent condensation probability, Phys. Rev. E 70 (6) (2004) 061605.
[34] D. Bedeaux, S. Kjelstrup, Transfer coefficients for evaporation, Phys. A: Stat. Mech. Appl. 270 (3–4) (1999) 413–426.
[35] C.A. Ward, The rate of gas absorption at a liquid interface, Chem. Phys. 67 (1) (1977) 229–235.
[36] L. Onsager, Reciprocal relations in irreversible processes, I, Phys. Rev. 37 (4) (1931a) 405.
[37] L. Onsager, Reciprocal relations in irreversible processes. II, Phys. Rev. 38 (12) (1931b) 2265.
[38] E. Johannessen, D. Bedeaux, Integral relations for the heat and mass transfer resistivities of the liquid–vapor interface, Phys. A: Stat. Mech. Appl. 370 (2) (2006) 258–274.
[39] J.-M. Simon, D. Bedeaux, S. Kjelstrup, J. Xu, E. Johannessen, Interface film resistivities for heat and mass transfers integral relations verified by non-equilibrium molecular dynamics, J. Phys. Chem. B 110 (37) (2006) 18528–18536.
[40] J.D. Van der Waals, The thermodynamic theory of capillarity under the hypothesis of a continuous variation of density, J. Stat. Phys. 20 (2) (1979) 200–244.
[41] E. Wild, On boltzmann's equation in the kinetic theory of gases, in: Mathematical Proceedings of the cambridge Philosophical society, volume 47, Cambridge University Press, 1951, pp. 602–609.
[42] H. Hertz, Ueber die verdunstung der flüssigkeiten, insbesondere des quecksilbers, im luftleeren raume, Ann. Phys. 253 (10) (1882) 177–193.
[43] M. Knudsen, Die maximale verdampfungsgeschwindigkeit des quecksilbers, Ann. Phys. 352 (13) (1915) 697–708.
[44] R.W. Schrage, A theoretical study of interphase mass transfer, Columbia University Press, 1953.
[45] O. Aydin, M.Y. Yassikaya, Validity and reliability analysis of the plotdigitizer software program for data extraction from single-case graphs, Perspect. Behav. Sci. (2021) 1–19.
[46] I.H. Bell, J. Wronski, S. Quoilin, V. Lemort, Pure and pseudo-pure fluid thermophysical property evaluation and the open-source thermophysical property library coolprop, Ind. Eng. Chem. Res. 53 (6) (2014) 2498–2508.
[47] W. Wagner, A. Pruß, The IAPWS formulation 1995 for the thermodynamic properties of ordinary water substance for general and scientific use, J. Phys. Chem. Ref. Data 31 (2) (2002) 387–535.
[48] M.L. Huber, R.A. Perkins, D.G. Friend, J.V. Sengers, M.J. Assael, I.N. Metaxa, K. Miyagawa, R. Hellmann, E. Vogel, New international formulation for the thermal conductivity of h2o, J. Phys. Chem. Ref. Data 41 (3) (2012) 033102.
[49] A.J. Queimada, C. Miqueu, I.M. Marrucho, G.M. Kontogeorgis, J.A.P. Coutinho, Modeling vapor–liquid interfaces with the gradient theory in combination with the CPA equation of state, Fluid Ph. Equilibria 228 (2005) 479–485.

[50] M. Sega, G. Horvai, P. Jedlovszky, Microscopic origin of the surface tension anomaly of water, Langmuir 30 (11) (2014) 2969–2972.
[51] Ø. Wilhelmsen, T.T. Trinh, S. Kjelstrup, D. Bedeaux, Influence of curvature on the transfer coefficients for evaporation and condensation of lennard-jones fluid from square-gradient theory and nonequilibrium molecular dynamics, J. Phys. Chem. C 119 (15) (2015) 8160–8173.
[52] J. Ge, S. Kjelstrup, D. Bedeaux, J.-M. Simon, B. Rousseau, Transfer coefficients for evaporation of a system with a lennard-jones long-range spline potential, Phys. Rev. E 75 (6) (2007) 061604.
[53] M.A. Kazemi, C.A. Ward, Contribution of thermocapillary convection to liquid evaporation, Int. J. Heat Mass Transf. 164 (2021) 120400.
[54] C.A. Ward, D. Stanga, Interfacial conditions during evaporation or condensation of water, Phys. Rev. E 64 (5) (2001) 051509.
[55] R. Savino, D. Paterna, N. Favaloro, Buoyancy and marangoni effects in an evaporating drop, J. Thermophys. Heat Trans. 16 (4) (2002) 562–574.
[56] G. Nagayama, T. Tsuruta, A general expression for the condensation coefficient based on transition state theory and molecular dynamics simulation, Chem. Phys. 118 (3) (2003) 1392–1399.
[57] B.-Y. Cao, J.-F. Xie, S.S. Sazhin, Molecular dynamics study on evaporation and condensation of n-dodecane at liquid–vapor phase equilibria, Chem. Phys. 134 (16) (2011) 164309.